4 EJIL - LAETA Young Researchers Meeting
AeroG, Covilhã, 9-10 November 2017

OPERATIONAL SAFETY SYSTEMS FOR SMALL DRONES

André C. Marta[a*], Alexandra B. Moutinho[a], Pedro V. Gamboa[b]

a) IDMEC - LAETA, Avenida Rovisco Pais 1, 1049-001 Lisboa
b) AeroG - LAETA, Calçada Fonte do Lameiro, 6201-001 Covilhã

* e-mail: andre.marta@tecnico.ulisboa.pt

Key words: Unmanned Aerial Vehicle, Flight Energy Management, Mission Planning, Obstacle Detection, Obstacle Avoidance

Abstract. *Recent incidents involving small drones have been raising concerns about their safe operation. It is foreseen that embedded safety systems will become mandatory in the near future, when stricter operational regulations will be put into place.*

This work is part of the on-going research aimed to address the current lack of intrinsic safety systems by developing three distinct but highly coupled subsystems: flight energy management (FEM), obstacle detection (OD) and mission planning (MP).

The FEM is able to estimate the energy balance of the updated mission plan by making an assessment of the available energy, both stored and to be harvested in-flight (e.g., photovoltaic), and comparing it to the required energy, taking into account the aircraft performance and in-route weather conditions (e.g., wind and solar radiation). This energy balance is continuously updated in real-time. The OD addresses all aspects of obstacle detection, namely the identification of the required aircraft instrumentation and the respective measurements processing to assess if there is probability of collision. Preliminary work using a LIDAR shows this sensor is valid for detecting close range obstacles. Further work will include its integration with other visual information in order to increase the detection range. Lastly, the MP allows for both pre-flight mission planning as well as in-flight mission replanning, taking into account the data received from the FEM to attest the mission feasibility, and from the OD regarding the detection of new obstacles. The mission planning depends on a set of desired waypoints, a list of known obstacles (static, such as terrain and buildings, or dynamic, such as other aircraft), the vehicle performance capabilities and the rules of air, resulting in a well-defined reference path. This path can currently be optimized for different metrics, such as time (minimum for fast execution or maximum for extended endurance), distance (maximum for extended range) or energy (minimum for extended range).

These three subsystems are meant to be integrated into the drone flight-controller to provide valuable data to the operator and, as a last resort, to automatically take action to avoid collisions or abort energy limited missions. A solar powered unmanned fixed wing aircraft, previously designed and built, will serve as one of the flight platforms to assess the operational capabilities of the developed safety subsystems. This vehicle has been flight tested to characterize its power requirements across the flight envelope thus providing key data used in the implemented algorithms' simulations.

1 INTRODUCTION

According to the Teal Group [1], drones, also known as Unmanned Aerial Vehicles (UAVs) and Remotely Piloted Aircraft (RPA), are, and will continue to be, the sector in the world aerospace industry that exhibit the largest growth in the current decade. The spending is forecast to increase from $6.4 billion annually to $11.5 billion in the next ten years, totalling almost $91 billion in the next ten years. This tremendous growth will also see a shift of the cumulative civil market from 11% to 14% by the end of 2024.

While the development of drones emerged in the military industry as vehicles designed to perform dangerous missions, the proliferation of UAV technology and the cascading down effect, contributed decisively to their application to civil missions. In recent years, the development of small low-cost drones, made the hobbyist market the largest consumer of such vehicles, with sales forecasted by the Federal Aviation Administration to be in excess of one million units in the USA alone in Christmas 2015 [2]. Among the top-three small UAVs manufacturers, that include Chinese DJI, French Parrot and US 3DRobotics, only very recently the former made available a somewhat limited obstacle sense and avoid system.

Being these low cost small drones at easy reach to the consumer, most often than not without any prior knowledge on how to operate such vehicles, there has been a very well-founded concern about the safety of people and property in the vicinity of drones. The goal of this project is to work towards the development of low cost safety systems that can be easily embedded in current hobby UAV platforms. These systems are meant to assist the operator by providing information concerning the vehicle status in terms of capability to perform the mission and, ultimately, automatically override the operator controls to avoid any catastrophic event.

2 OPERATIONAL SAFETY SYSTEM

This work is part of the Safe Drones research project aimed to address the current lack of an intrinsic safety system by developing three distinct but highly coupled subsystems: flight energy management (FEM), obstacle detection (OD) and mission planning (MP). These subsystems are tightly coupled to each other, as shown in Fig.1.

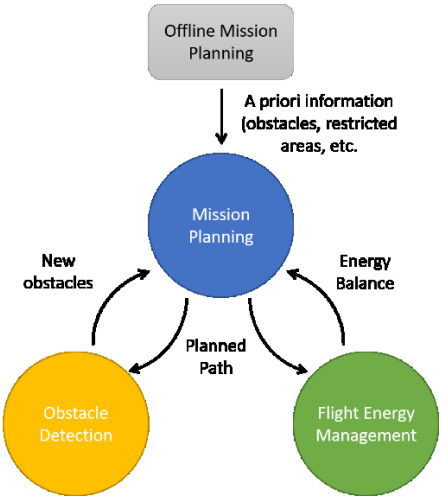

Figure 1: Operational safety system [3].

The interaction between these three subsystems aims to enhance low-cost UAV safety. Any flight should start with offline mission planning, accounting for known obstacles, restricted areas, limited autonomy and any other relevant a priori information. Given the planned path, the obstacle detection module evaluates possible collision threats in real time, and if an evasive manoeuvre has to be performed, the mission planning module recalculates a possible flight path. Simultaneously, the energy management module evaluates the expected energy balance up to the landing point, and if it is negative, a new mission path must be recalculated. Notice however that, at these early stages of the project, each subsystem is being developed as an individual module, assuming the input data to be provided by the outputs of other modules is available.

The following sections describe the complete work and the achievements obtained regarding the MP and FEM modules, and remarks are made about the OD module yet to be developed.

3 MISSION PLANNING

Path planning with obstacle avoidance is a fundamental aspect of autonomous vehicles operations. To this day, several solutions have been developed to tackle this problem. The proposed methods so far are divided into two main categories: global and local path planning. Global path planning requires a known static environment and is generally performed offline before the mission begins. Local path planning methods are implemented during mission execution and are responsible for the replanning of the original path when new obstacles are detected.

Graph search algorithms are one of the most popular methods used in robot path planning. These methods are heavily based on the Dijkstra's algorithm [4] where starting at one vertex a graph is searched by exploring adjacent nodes until the goal state is reached, with the intent of finding the optimal path. In [5] a variation of the A* algorithm is proposed for path planning of fixed-wing UAVs in 3D environments, providing a feasible solution for offline path planning with turning and climbing angles constraints. The Ant Colony Optimization algorithm has also been applied to the UAV global path planning problem [6]. The solutions however are only applied to 2D environments, considering a constant flying height, which is not suitable for many applications of flying vehicles. The Artificial Potential Field methods are an approach inspired by physical potential fields. These methods are generally used for reactive collision avoidance systems [7] and are a good solution for online implementation.

This work presents a two-stage path planning architecture. In the first stage, the global planning module, which assumes a known static environment, determines a collision free path from a given start to goal configurations. This path is given as a reference for the mission execution stage and as new threats are detected by the on-board sensors, the local planning module must replan the path to avoid these new obstacles.

Figure 2 illustrates the proposed framework for the path planning system and its integration with the other system modules. The navigation module is responsible for the estimation of the UAV state, which comprises its position and velocity. The obstacle detection module contains the sensors and algorithms necessary to detect and estimate the obstacles state. In this work, the type of sensors used will not be specified, but it is assumed that there is a working method of sensor fusion to obtain the necessary

information about the environment. For the purpose of collision avoidance, a safety volume is defined around the obstacles. Due to its simplicity and ability to encompass a wide variety of obstacle types, a cylindrical model is used to represent obstacles.

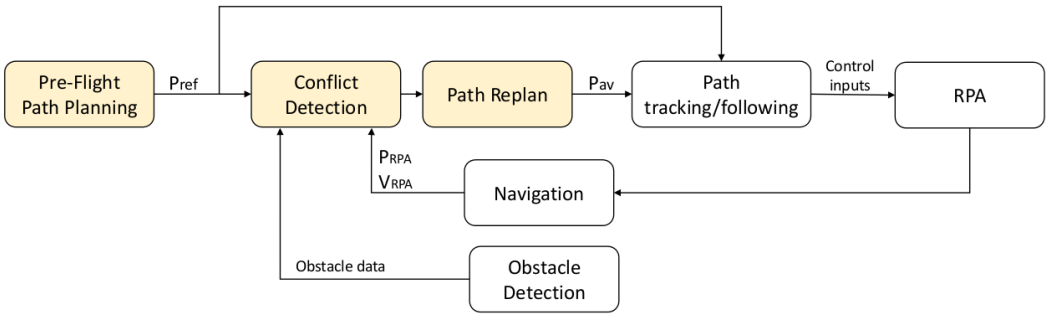

Figure 2: System architecture [8].

3.1 Pre-Flight Path Planning

In this work, the configuration space will be defined as a regular grid. Some of the kinematic constraints of the vehicle, minimum turning radius and maximum climb angle, were included in the definition of the search space. Other constraints in the vehicle maneuverability can be included in the process of node expansion during the search process through the graph.

Distinct expansion rules are defined for multirotor and fixed-wing platforms. Fixed-wing platforms have a forward only motion and cannot make sharp turns or climbs. To incorporate maneuverability restrictions, a set of expansion rules is defined as seen in Fig.3.

Figure 3: Expansion rules for fixed-wing aircraft [8].

Other constraints include the minimum safety distance, given the relative distance between the UAV position and the obstacle.

Depending on the mission objectives, different cost functions can be considered. For the minimum distance paths the cost function is simply given by the sum of Euclidean distance between all points. Considering a path $\boldsymbol{P}$ of N waypoints, the cost is given by

$$F_d = \sum_{i=1}^{N-1} \|\boldsymbol{P}_{i+1} - \boldsymbol{P}_i\| \tag{1}$$

To formulate the energy minimization problem, an energy balance is considered. Considering a point mass model for the UAV, its motion can be analysed using the work and energy method. The energy balance is a statement about how energy is spent when the UAV moves from point i to point j,

$$E_{i\to j} = \frac{1}{2} m \left(v_j^2 - v_i^2\right) + D\Delta s + mg\Delta h \tag{2}$$

where m is the UAV mass, v the vehicle speed, D the drag force, s the air displacement, g the gravity component and h the height variation. The cost function for minimum energy paths is then given by

$$F_e = \sum_{i=1}^{N-1} E_{i \to i+1} \tag{3}$$

The A* algorithm [4] works by systematically searching the graph by applying the transition function and choosing the states that minimize the cost function. The Ant Colony Optimization (ACO) [5] is a metaheuristic method derived from the observation of real ant's behaviour that uses a pheromone trail to mark paths from the nest to the food source. The paths obtained with A* and ACO consist of straight line segments between waypoints. These paths cannot be exactly followed by the UAV with dynamic and kinematic constraints. Bezier curves are used to generate a flyable path for the UAV. Bezier curves are a type of parametric curves designed to provide a smooth path that passes exactly through the initial and final waypoints and is influenced by the other waypoints on the way, which are defined as control points. A particular case of these curves are Rational Bezier curves [9], given by

$$P_R(t) = \frac{\sum_{i=0}^{n} B_i^n(t) \cdot w_i \cdot P_i}{\sum_{i=0}^{n} B_i^n(t) \cdot w_i}, \; t \in [0,1] \tag{4}$$

where $B_i(t)$ is the Bernstein polynomial, P_i the control points given, by A* and ACO, and w_i the curve weights. The curvature of a parametric curve $P(t)$ can be calculated as

$$k(t) = \frac{|P'(t) \times P''(t)|}{|P'(t)|^3} \tag{5}$$

The defined problem is to optimize the weights of a rational Bezier curve. The optimization problem is formulated as

$$\begin{aligned} \text{minimize} \quad & F_C \\ \text{subject to} \quad & d_0 \geq R_s \\ & P_R(t) = f(w) \\ & |k| \leq k_{max} \\ & w_{min} \leq w_i \leq w_{max} \end{aligned} \tag{6}$$

The cost function F_c to be minimized is given either by Eq.(1) or Eq.(3). If the constraints are to be satisfied without optimizing the cost function F_c is set to zero. The constraints impose a minimum distance between the UAV and the obstacle, and ensure that, given the UAV turning limits, the path is flyable.

All the following examples were obtained with MATLAB R2016a running on an Intel Core i5 with a CPU of 2.4 GHz, 4Gb RAM and Windows 7.

In Fig.4, a minimum energy path is planned in the presence of a wind field. The figure also shows the UAV departure heading. The presented results are obtained with the A* algorithm, which provided better results than ACO. Three curves determined from the A* points, P_i, are also depicted: B_i (the initial Bezier curve with unitary weights), B_c (the curve with adjusted weights to satisfy constraints) and B_o (the curve obtained from constrained optimization of the cost function).

From the results in Tab.1, it is seen that the optimized Bezier curve provides the path of minimum cost, but it has a longer computation time and provides little improvement over the curve that is only computed to satisfy constraints.

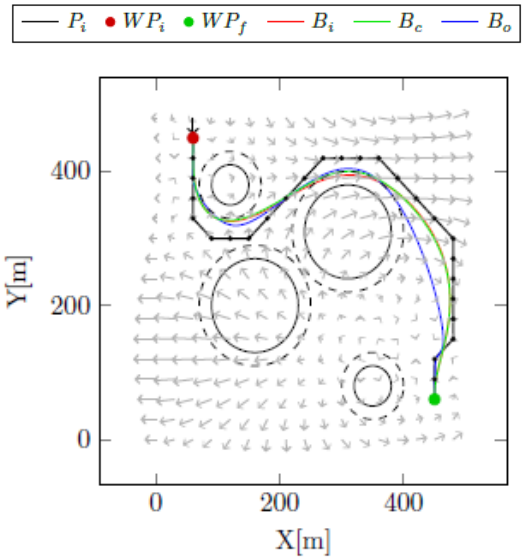

Figure 4: Minimum energy paths for fixed-wing platform using the A* algorithm [8].

Table 1: Minimum energy for 2-waypoints.

Path	Energy (kJ)	CPU time (s)
A^*	4.02	0.120
B_i	3.50	0.027
B_c	3.51	11.91
B_o	3.43	79.84

3.2 Real-Time Path Planning

This section tackles the problem of replanning a reference path when new obstacles are detected, while considering the Rules of the Air [10]. The time to collision, t_{CPA}, is used, thus higher priority will be given to intruders with the smallest t_{CPA} and the conflicts are resolved in a sequential manner.

The Potential Fields approach is used, where the obstacles and the goal position are treated as charged particles [7]. A repulsive force is attributed to the obstacles and an attractive force to the goal point. The sum of those forces is used to generate the direction of motion. The proposed fields are generated in a similar way to [11]. From the total field vector, the required heading and flight path angles to avoid the obstacle are obtained, from which, knowing the current direction of motion, a series of waypoints are generated until the obstacle has been cleared.

A set of situations are presented where a segment of the original path must be replanned to avoid new obstacles. The first case represents a UAV that is on a climbing trajectory when a moving intruder is detected. The replanned path leads to the levelling off the UAV, as depicted in Fig.5, to avoid the obstacle. The replanning computation time took 0.019s.

Another example shows a moving obstacle blocking one of the points of obligatory passage. As seen in Fig.6, the UAV follows the right-hand rules to avoid the obstacle without compromising the safety distance. This computation required 0.015s of CPU time. Again, the computation time of the online stage is fast enough to be suited for real-time implementation.

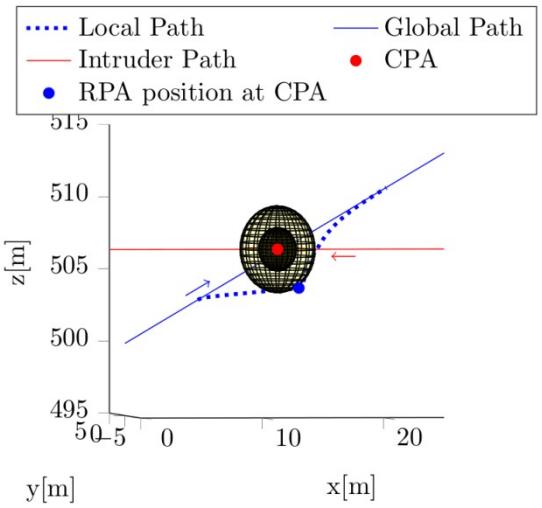

Figure 5: Converging encounter [8].

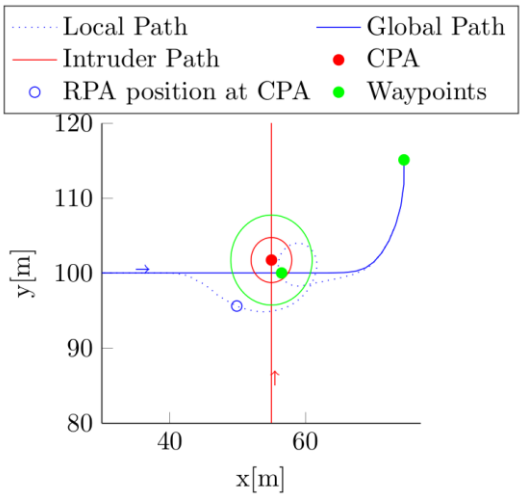

Figure 6: Converging encounter with missed waypoint [8].

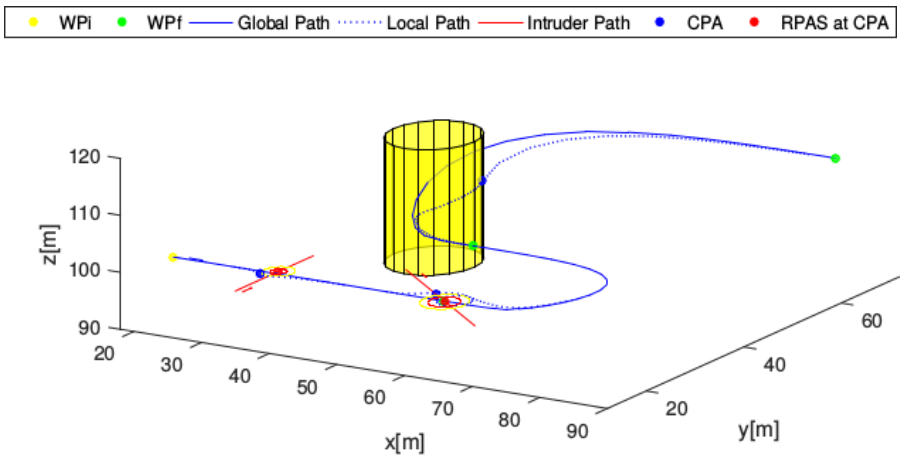

Figure 7: 3D path with multiple obstacle avoidance [8].

In the final example, the UAV encounters two moving intruders, with one of them blocking a reference waypoint, and a static obstacle while following the reference path. The resulting replanned path is depicted in Fig.7.

3.3 Remarks

This module was aimed to provide autonomous flight capabilities to UAVs with collision avoidance capabilities. The task was divided into a global and a local layer.

For the global path planning stage the best results were found to be provided by a combination of the two algorithms, using A* and ACO to optimize waypoint order. The global planner can resolve a series of different scenarios and new optimization criteria can be easily added to expand the range of problems to be solved.

For the online stage, Potential Fields are used to generate a local trajectory when unknown obstacles are detected. The replanning of the path is made considering an uncooperative situation between the vehicles, and a sequential resolution of encounters, prioritized according to time to collision. The Potential Fields method is computationally inexpensive being a feasible solution for real-time implementation.

4 FLIGHT ENERGY MANAGEMENT

The energy management (or energy monitoring) module is responsible for assessing the energy requirements and expected energy balance for the assigned mission, and for the aircraft's safe return to base, accounting for meteorological conditions experienced such as wind and solar radiation.

The goal is to develop a system capable of generating an updated estimate of the state of total energy remaining onboard the aircraft at the end of the mission (the margin remaining in terms of energy), capable of being run on the airborne avionics hardware, enabling better energy awareness when planning a mission or advising a mission adjustment or a return to base if the energy margin drops below a defined safe value. The first estimation is done pre-mission (offline) and later the update of the estimate is periodic as the mission progresses (online), taking into account the conditions experienced (wind, solar radiation, handicapped airframe or trajectory change, either due to a pilot or ground control command or automatic obstacle avoidance manoeuvres), as well as those predicted for the remainder of the mission.

4.1 Energy Estimation Models

Figure 8 provides an overview of how the estimation of the remaining energy at the end of the flight is obtained.

The past energy flow analysis starts with the initial state of the system, the energy available in all energy sources at the start of the mission $E_{sources,t0}$, then the energy flowing out of the system (measured consumed energy) is subtracted, $E_{cons,t\_0\rightarrow t}$, and the energy harvested (flowing into the system) $E_{solar|harv,t0\rightarrow t}$ is added. This results in the energy available in the energy sources in the present (at time instant *t*),

$$E_{sources,t}(t) = E_{sources,t_0} + E_{solar|harv,t_0\rightarrow t}(t) - E_{cons,t_0\rightarrow t}(t) \quad (7)$$

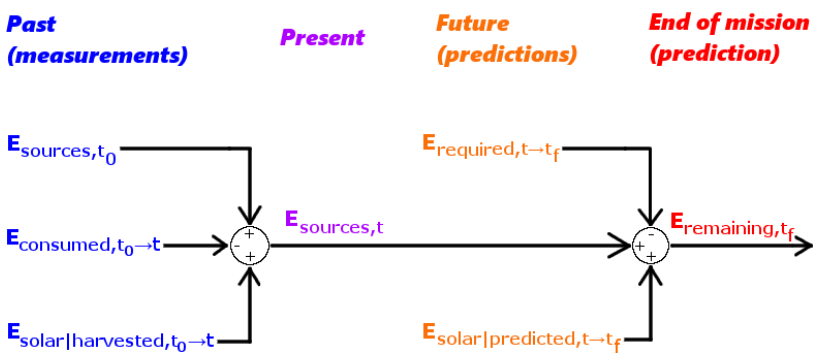

Figure 8: Energy balance at end of mission [3].

To obtain the future energy flow, the expected energy to flow out of the system in the future (required energy to complete the mission) $E_{req,t\rightarrow tf}$ is subtracted, and the expected energy to flow into the system in the future (solar energy expected to be harvested in the remainder of the mission) $E_{solar|pred,t\rightarrow tf}$ is added. This results in the estimated final state of the system, the estimated remaining energy in the sources at the end of the mission

$$E_{rem,t_f}(t) = E_{sources,t}(t) + E_{solar|pred,t\rightarrow t_f}(t) - E_{req,t\rightarrow t_f}(t) \tag{8}$$

The energy available in the energy sources at the start of mission is modelled by

$$E_{sources,t_0} = E_{battery,t_0} + E_{fuel,t_0} + E_{p,t_0} + E_{k,t_0} \tag{9}$$

where $E_{battery,t0}$ and $E_{fuel,t0}$ are the energy available in the battery and in the fossil fuel tank at the start of the mission respectively, and $E_{p,t0}$ and $E_{k,t0}$ are the potential and kinetic energies of the aircraft at the start of the mission, respectively. The initial energy stored in the battery is given by

$$E_{battery,t_0} = 3600\, SoC\, Q_{nom} U_{nom} \tag{10}$$

where SoC is the state of charge of the battery (between 0 and 100%), Q_{nom} is the nominal charge of the battery and U_{nom} is the nominal voltage of the battery. The initial energy contained in the fuel tank is related to the volume of fuel it contains,

$$E_{fuel,t_0} = u_{fuel} m_{fuel,t_0} = u_{fuel} \rho_{fuel} V_{fuel,t_0} \tag{11}$$

where u_{fuel} is the specific energy of the fossil fuel, ρ_{fuel} is its density and $V_{fuel,t0}$ is its volume at the beginning of the mission.

The model for the energy consumed is given by

$$E_{cons,t_0\rightarrow t}(t) = \int_{t_0}^{t} \dot{E}_{battery}(t)dt + \int_{t_0}^{t} \dot{E}_{solar|harv}(t)dt + \int_{t_0}^{t} \dot{E}_{fuel}(t)dt \tag{12}$$

where the terms are estimated as

$$\int_{t_0}^{t} \dot{E}_{battery}(t)dt = \int_{t_0}^{t} U_B I_B dt \tag{13}$$

and

$$\int_{t_0}^{t} \dot{E}_{fuel}(t)dt = u_{fuel}\rho_{fuel} \int_{t_0}^{t} \dot{V}_{fuel} dt \tag{14}$$

where $\dot{V}_{fuel}$ is the fuel volumetric flow. This assumes that the quantities U_B, I_B, U_{PV}, I_{PV} and $\dot{V}_{fuel}$ are measured. It is important to notice that I_B can be both positive or negative, depending on whether the battery is being discharged or charged, respectively. The solar energy harvested from the beginning of the mission until time instant t is described by

$$\int_{t_0}^{t} \dot{E}_{solar|harv}(t)dt = \int_{t_0}^{t} U_{PV} I_{PV} dt \tag{15}$$

The required energy to complete the mission is obtained by estimating the future consumption of the propulsion system $E_{prop,t\rightarrow tf}$, the future consumption of all the avionics equipment $E_{av,t\rightarrow tf}$ and also taking into account the change in mechanical energy (ΔE_p and ΔE_k) between the instant of calculation t and the end of the mission,

$$E_{req,t\rightarrow t_f}(t) = \Delta E_p(t) + \Delta E_k(t) + E_{av,t\rightarrow t_f}(t) + E_{prop,t\rightarrow t_f}(t) \tag{16}$$

To estimate the required propulsion energy to finish the mission successfully two different approaches were considered. The first approach (M1) is based on the force diagram of Fig.9 (for a generic aircraft), from which the required thrust is obtained.

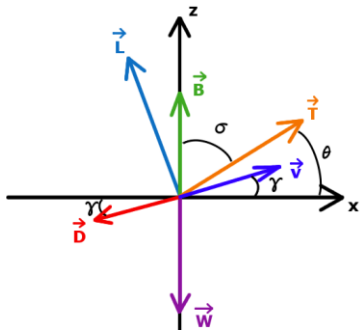

Figure 9: Force diagram for a generic aircraft [3].

The balance of forces is therefore given by

$$\begin{cases} L - W\cos(\gamma) + B\cos(\gamma) + T\sin(\alpha) = 0 \\ T\cos(\alpha) - D - W\sin(\gamma) + B\sin(\gamma) = ma \end{cases} \tag{17}$$

where B represents the buoyancy force. The drag polar curve $C_D=f(C_L)$ and the relationship between lift coefficient and the angle of attack $C_L=f(\alpha)$ of the aircraft are used in addition to Eq.(17) to solve the balance of forces, assuming the desired acceleration for each mission segment, the weight and buoyancy (in case the aircraft in study is an airship) of the aircraft are known. Air density ρ is modelled according to the Earth's atmosphere standard model of reference and the climb angle γ is calculated according to the waypoints defined during mission planning.

The second approach (M2) to determine the required propulsion and avionics power required is to experimentally characterize the energy requirements of an aircraft as a function of airspeed, exemplified in Fig.10 for the LEEUAV [12] in cruise condition.

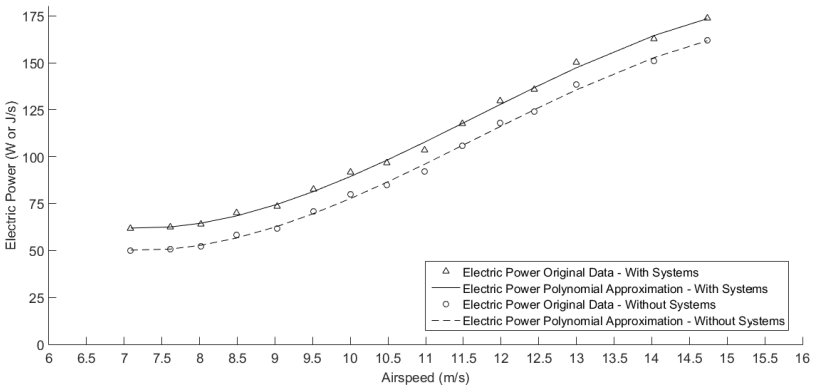

Figure 10: Power required as function of airspeed for the LEEUAV in cruise [13].

The required propulsion energy to finish the mission can then be obtained by integrating the corresponding value of required electric power P_{el} from the curve over the expected remaining duration of the mission,

$$E_{av,t\to t_f}(t) + E_{prop,t\to t_f}(t) = \int_t^{t_f} P_{el} dt \tag{18}$$

Assuming level flight (which constitutes the largest percentage of mission time), the approach in [14] can be used to estimate the solar irradiance in a given location, at a given time. The expected energy to be harvested from a given time instant *t* until the end of the mission is finally obtained by integrating the power output of the solar panel over time,

$$E_{solar|pred} = \int_t^{t_f} J S_{PV} \eta_{PV} dt \tag{19}$$

where *J* is the solar radiance (solar power per unit area), S_{PV} is the solar panel area and η_{PV} is its efficiency.

4.2 Simulation Results

Offline simulations were performed for the case of the LEEUAV, given the available data from previous works (polar curve, relationship between lift coefficient and angle of attack, and Fig.10), to assess the performance of the FEM in this case. The offline simulations aim to predict if the planned mission is feasible (before take-off). The mission profile and ground speed profile are shown in Fig.11.

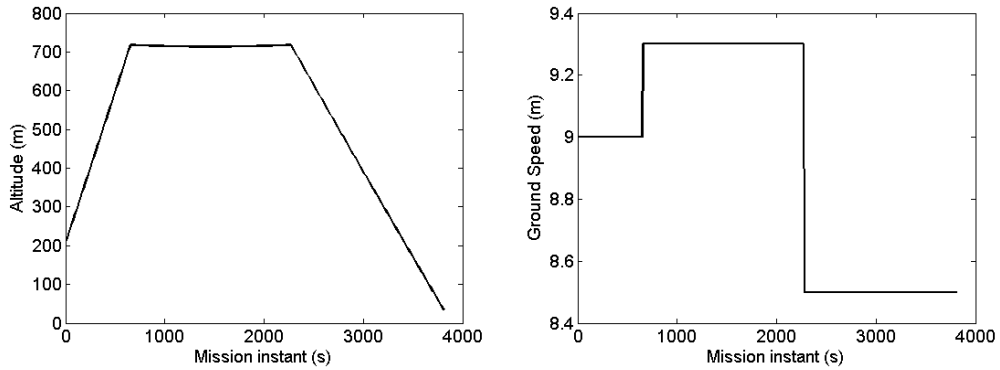

Figure 11: Power required as function of airspeed for the LEEUAV in cruise [3].

An initial simulation without wind was performed to compare the predicted propulsion power requirements for different flight stages using each method used to estimate the required energy to complete the mission, and the results are shown in Tab.2.

Method 2 is very accurate at predicting the power required to fly during cruise, since it derives from an experimental characterization. This means that method 1 overestimates the power requirements for cruise by approximately 106%, which is not good. Method 2 on the other hand, severely underestimates the power requirements for climb, since the experimental characterization on which method 2 is based on was performed only for the cruise condition, and no data was available for climb. The required power for the descent stage is zero since it is assumed the aircraft glides while descending. These results show that these methods are sensitive to the quality of the data available to perform the estimates.

Table 2: Predicted propulsion power (W) required to fly each stage by each method.

Stage	M1	M2
Climb	578.3	247.1
Cruise	132.8	64.4
Descent	0.0	0.0

For the following simulations, an arbitrary temporal wind profile was chosen as shown in Tab.3, in which the mission instants indicate when the respective wind speed changes to that value.

Table 3: Wind temporal profile.

Mission instant (s)	Wind speed (m/s)
0	1.2
600	0.8
1200	1.9
1800	1.5
2400	0.3
3000	0.7
3600	0.6
4200	1.0

The influence of performing the mission in different days of the year (day 172 - Summer Solstice, and day 355 - Winter Solstice) and different starting hours was also investigated. The results obtained are shown in Tab.4.

Table 4: Energy estimated from offline simulations.

Energy (kJ)	Day 172, 9h	Day 172 15h45	Day 355 9h
$E_{sources,t0}$	408.9	408.9	408.9
E_{req} *M1*	836.6	836.6	836.6
E_{req} *M2*	382.6	382.6	382.6
$E_{solar\|pred}$	627.2	428.6	263.0
E_{rem} *M1*	199.5	1.0	-164.6
E_{rem} *M2*	653.5	454.9	289.3

Two main conclusions can be drawn from Tab.4. First it is possible to observe that during the Summer Solstice more solar energy is expected to be harvested compared to the Winter Solstice when the mission begins at the same hour, which makes sense. Also, on the same day more energy is expected to be collected if the mission starts in the morning than if it starts later in the afternoon, which is also a result to be expected. It is predicted that the mission can be completed safely in the Summer Solstice if it starts at 9h, and the battery would still have around 50% of its total energy at the end. If the mission starts at 15:45h however, the battery is predicted to finish the mission with less than 1% of its total energy, which is a value low enough to raise safety concerns, and the mission should be replanned. During the Winter Solstice, the value of remaining energy is negative, meaning that the battery does not have enough energy to complete this mission, since not enough solar energy would be collected to compensate the amount consumed. If method 2 is used instead to calculate the required propulsion power, then the conclusion would be that this mission could be completed safely in any of the conditions considered. In reality, this probably would not be true since, given the available data, the power requirements for climb would be underestimated by method 2. With better data available, this method would be more useful and provide more accurate remaining energy estimates.

5 FLIGHT PLATFORMS FOR SYSTEM TESTING

The work now being developed is built on a previous project of a Long Endurance Electric Unmanned Aircraft Vehicle (LEEUAV), that included the collaboration of research groups IDMEC at Instituto Superior Técnico and AEROG at Universidade da Beira Interior) [12], both part of LAETA. The goal was to develop a low cost, small footprint electric UAV, capable of being deployed from short airfields, easy to build and maintain, and highly flexible to perform different civilian surveillance missions. The resulting design is illustrated in Fig.12.

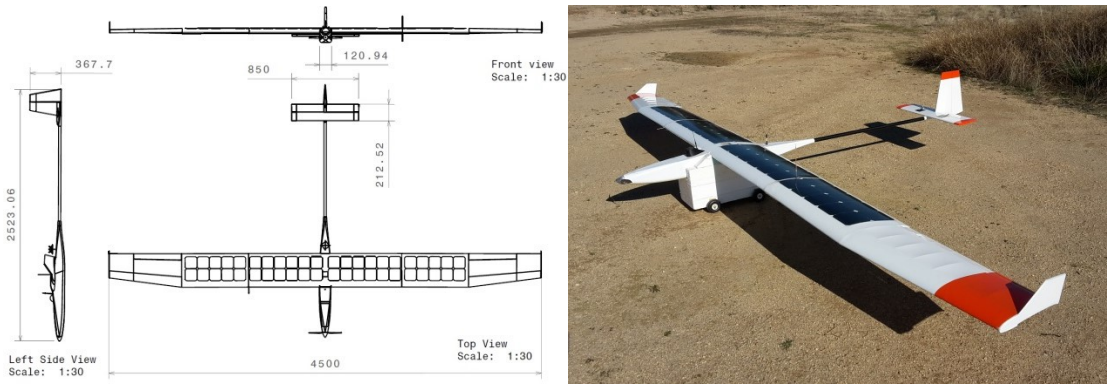

Figure 12: Flight platform LEEUAV [13].

Through this legacy project, some important lessons were learnt by addressing key design tasks: 1) several different electric propulsion system configurations were evaluated in terms of performance, overall weight and cost. It led to the selection of high-efficiency photovoltaic solar panels, high-density rechargeable batteries and combination of propeller with brushless electric motor [15]; 2) using high-fidelity CFD analysis, the aerodynamic design of the airframe, including wing, fuselage and tail, was modelled. The computational process put in place enables the swift design of different UAV configurations [16]; 3) the autopilot and First Person View (FPV) hardware and software were selected and tested in flight to assess its long range capability [17].

The prototype was designed and built, using advanced model building techniques, and test flown, both radio control operated [18] and autonomously operated with the full set of communications, FPV and solar harvesting systems [13].

6 CONCLUSIONS

Two safety subsystems targeted for low-cost UAVs were developed: the mission planning (MP), both pre-flight and real-time, and the flight energy management (FEM). Their capabilities were demonstrated in simulations, being planned their integration in an existing flying platform. However, prior to that integration, the development of the obstacle detection (OD) subsystem is paramount.

In terms of MP, it was demonstrated that optimal obstacle-free paths could be obtained using a combination of both ACO and A* algorithms. As these were computed pre-flight, the associated computational cost is justified by the accuracy of the results. As for the real-time replanning, it was also demonstrated that the potential field approach is very efficient in providing a modified path to avoid new obstacles while obeying the rules of air, at a reduced computational cost, which makes it suitable for embedding in on-board control systems.

Relative to the FEM developed, the energy balances considered can tackle any type of aircraft (fixed- or rotary-wings) and several propeller-driven propulsion systems (combustion or electric) and a combination of energy sources (fuel, batteries and solar). It was seen that the results are highly sensitive to the aircraft performance data and propulsion system characterization. As such, these must be carefully handled and tuned for each particular UAV during testing of the system.

Even though the described fixed wing platforms were the drivers for the current project, the safety systems developed are intended to be general in application, so that they can be embedded not only in fixed wing platforms but also rotary wing platforms (e.g. multicopters).

The next effort will focus on the sensor hardware development for obstacle detection. A combination of sonar and LIDAR is meant to provide both accurate short-range and coarse long-range capabilities, respectively. Further work will include their integration with other visual information to increase the detection range.

ACKNOWLEDGEMENTS

This work was supported by FCT (Foundation for Science and Technology) through IDMEC, under LAETA, project UID/EMS/50022/2013. The work presented is sponsored by LAETA to leverage the multi-disciplinary competences among its several research centres, particularly in the area of Aeronautics.

The project benefited greatly from the collaboration of master students, in particular, Juliana Alves, Tiago Baião, Pedro Moutinho, Eduardo Pinho and Afonso Rodrigues, to whom the authors thank for their effort and dedication.

REFERENCES

[1] Teal Group. World Unmanned Aerial Vehicle Systems, Market Profile and Forecast 2014.

[2] A. Karp. FAA Nightmare: A million Christmas drones, Aviation Daily, Sep 28, 2015.

[3] T. Baião. Energy monitoring system for low-cost UAVs, Master's thesis, Instituto Superior Técnico, Lisboa, Portugal, July 2017.

[4] E.W. Dijkstra. A note on two problems in connexion with graphs. *Numerische Mathematik*, 1(1):269-271, 1959. doi:10.1007/BF01386390.

[5] L. Filippis, G. Guglieri, and F. Quagliotti. Path planning strategies for UAVs in 3D environments. *Journal of Intelligent and Robotic Systems*, 65(1):247-264, 2012. doi:10.1007/s10846-011-9568-2.

[6] C. Zhang, Z. Zhen, D. Wang, and M. Li. UAV path planning method based on ant colony optimization. In 2010 Chinese Control and Decision Conference, pages 3790-3792, May 2010.

[7] J. Ruchti et al. RPAS collision avoidance using artificial potential fields. *Journal of Aerospace Information Systems*, 11(3):140-144, 2014.

[8] J. Alves, Path planning and collision avoidance algorithms for small RPAS, MSc Thesis, Instituto Superior Técnico, Portugal, June 2017.

[9] D. Marsh. Applied Geometry for Computer Graphics and CAD. Springer-Verlag, London, 2ed., 2005.

[10] ICAO. Rules of the air. Annex 2 to the Convention on International Civil Aviation, 2005.
[11] D. Ruivo. Formation of unmanned vehicles with collision avoidance capabilities. Master's thesis, Instituto Superior Técnico, Lisboa, Portugal, Nov. 2015.
[12] A.C. Marta, P. Gamboa. Long endurance electric UAV, Proceedings of the ICAS 2014 Conference, St. Petersburg, Russia, Sep. 2014.
[13] A. Rodrigues, Airframe Assembly, Systems Integration and Flight Testing of a Long Endurance Electric UAV, Master's thesis, Universidade da Beira Interior, Portugal, Feb. 2017.
[14] G. Xian-Zhong, H. Zhong-Xi, G. Zheng, L. Jian-Xia, and C. Xiao-Qian. Energy management strategy for solar-powered high-altitude long-endurance aircraft. *Energy Conversion and Management*, 70:20-30, 2013. doi:10.1016/j.enconman.2013.01.007.
[15] M. Ferreira. Hybrid Propulsion of a long endurance electric UAV, Master's thesis, Instituto Superior Técnico, Portugal, Nov. 2014.
[16] N. Silva. Parametric Design, aerodynamic analysis and optimization of a solar UAV, Master's thesis, Instituto Superior Técnico, Portugal, Jun. 2014.
[17] P. Miller. Design of a remote person view system for a long range UAV, Master's thesis, Instituto Superior Técnico, Portugal, Jun. 2015.
[18] L. Cândido. Design of a long range solar UAV, Master's thesis, Universidade da Beira Interior, Portugal, Oct. 2014.